A UHV-ESR STUDY OF THE REACTION OF NO_2 ADSORBED ON COPPER

by Mark NILGES, Glenn BARKLEY,
Masaru SHIOTANI (*), and Jack H. FREED

Baker Laboratory of Chemistry
Cornell University
Ithaca, New York 14853

ABSTRACT

We describe in detail an experimental design which permits the high sensitivity study of ESR from paramagnetic species that may form on clean metal (and oxide) surfaces. The heart of the design is the ultra-high vacuum ESR cavity. The new phenomenon CREMSEE (cyclotron resonance from microwave-induced secondary electron emission), which is observed under high vacuum conditions, is characterized in some detail. In particular, it is found to be a sensitive indicator of surface bonding. The results of a detailed study of the reaction of NO_2 with Cu performed in the UHV-ESR system are presented. It is shown that the initial oxidation process may be monitored by CREMSEE, while an ESR signal is only seen when H_2O is present. The primary role of the H_2O is to form a hydrated surface copper complex which is magnetically concentrated but microcrystalline. These results are then compared with a study on supported Cu performed under conventional vacuum conditions.

RESUME

Les auteurs décrivent un appareillage pour l'étude par RPE avec une sensibilité élevée des espèces paramagnétiques susceptibles de se former sur des surfaces de métal ou d'oxydes. La partie importante de l'appareillage est une cavité RPE à ultra vide qui permet l'étude détaillée du nouveau phénomène de résonance cyclotron à partir d'émission électronique secondaire induite par microonde. Cet effet très sensible en particulier aux liaisons superficielles est appliqué à l'étude de la réaction de NO_2 sur le cuivre métallique effectuée dans la cavité RPE à ultravide. L'étape initiale d'oxydation peut être caractérisée par résonance cyclotron alors que le signal RPE n'apparaît qu'en présence d'eau. Le principal rôle de l'eau est de former un complexe superficiel du cuivre hydraté qui est magnétiquement concentré mais microcristallin. Ces resultats sont ensuite comparés à ceux obtenus dans le cas du cuivre supporté dans des conditions de vide conventionnel.

I. Introduction

In recent years there has been an increasing interest in developing surface spectroscopy in order to study the chemical bonding of adsorbed species to metal surfaces, since this is important in the study of catalysis and corrosion. Electron spectroscopies such as ultraviolet photoemission spectroscopy (1) (UPS) and high resolution electron loss spectroscopy (2) (EELS) are sensitive techniques but are limited in resolution. Conventional molecular spectroscopies such as infrared (3) and Raman (4) have been applied to the study of adsorption on metal surfaces. These techniques have high resolution and do not necessarily require that the surface be under vacuum, but they do have low sensitivity, especially for Raman, except under certain conditions of surface enhancement, and for IR when the adsorbate has a small or negligible dipole moment. IR has been applied to low surface area metal-adsorbate studies under ultra-high vacuum (UHV) conditions using various enhancement techniques (5) and more recently Raman spectroscopy has been performed under UHV conditions (6).

Electron spin resonance (ESR), like IR and Raman has high resolution, limited sensitivity under certain conditions, and can be observed at high pressures. While ESR is limited to the detection of unpaired electron spins, it focusses specifically on paramagnetic species such as atoms, ions, and free radicals, which are often involved in reactions at surfaces. Also transition metals can form paramagnetic complexes with adsorbed molecules by oxidation-reduction reactions. ESR has previously been applied to the study of surfaces (7-10), but only a few studies have been performed with supported metal surfaces (11) or surfaces prepared under UHV conditions (12-15), and no studies have previously been performed on metal surfaces prepared under UHV conditions.

We report results using a new technique for the in situ study of molecular adsorption and reactions of gases on metallic surfaces prepared under UHV conditions. In particular, we report the reaction of NO_2 adsorbed on a copper film, and the effect of coadsorption of other reactive species upon the corrosion of the copper surface. We compare these results with results of experiments obtained from the reaction of NO_2 with supported Cu to illustrate important differences.

We also report the observation of a new phenomenon: that of cyclotron resonance from microwave induced secondary electron emission (CREMSEE). This phenomenon appears to be useful for the study of adsorption on and/or characterization of metal surfaces.

We describe the UHV-ESR experimental design in Section II, and the CREMSEE phenomenon in Section III. Our study of the reaction of NO_2 with Cu films is summarized in Section IV; while the results of NO_2 on supported Cu are given in Section V. The conclusions appear in Section VI.

II. Experimental Design of UHV-ESR

A diagram of our UHV-ESR system is shown in Figure 1. The vacuum system is all stainless steel, except for the microwave cavity which is constructed of titanium. The system is roughed using a cryosorption pump and is pumped to UHV by a 50 l/sec ion pump and a titanium sublimation pump cooled to liquid nitrogen temperatures. The system has a base pressure of $2\text{-}4 \times 10^{-10}$ torr after bakeout to 150 °C. Leak valves were used to admit NO_2, and/or H_2O from an all stainless steel gas handling system. NO_2 was leaked into the cavity using a stainless steel dosing needle to avoid decomposition of NO_2 by the ion gauge and mass analyzer.

(*) Permanent Address: Faculty of Engineering
Hokkaido University
Sapporo 060, Japan

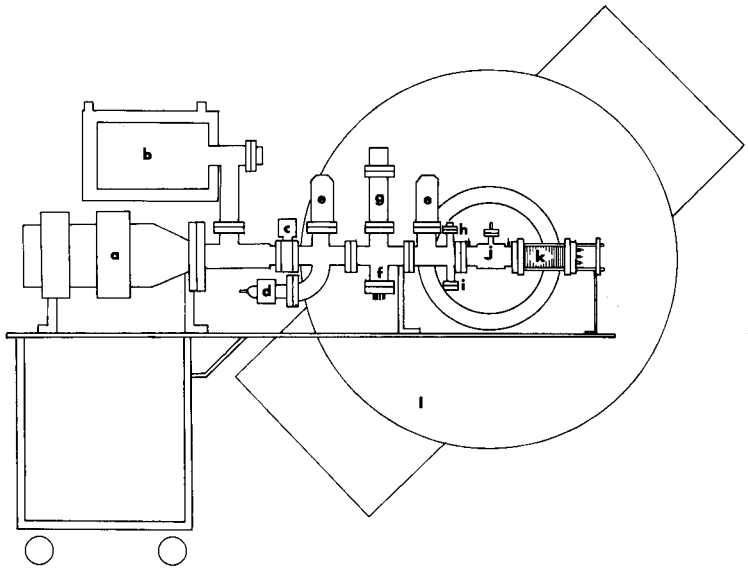

Fig. 1. — UHV-ESR System: a) ion pump, b) titanium sublimation pump, c) butterfly valve, d) cold cathode gauge, e) leak valves, f) ion gauge, g) mass analyzer, h) sapphire window, i) mirror mount, j) cavity, k) evaporator assembly, l) magnet.

Pressure measurement could be performed between 10^{-11} torr and 20 torr using a combination of a nude ionization gauge, a cold cathode gauge, a 1 to 10^3 millitorr thermocouple gauge, and a .1 to 20 torr thermocouple gauge. A capacitance manometer is used for calibration of the thermocouple gauges. A quadrupole mass analyzer is used for checking gas purity, leak checking, and examining desorption species. A silver-coated stainless steel mirror and a UV grade sapphire window may be used for photo-induced ESR studies.

The use of a 3KG magnetic field at X-band frequencies imposes many limiting factors which our design has minimized. The microwave cavity/vacuum system must fit into the 3" pole gap of the magnet. The materials used in the construction of the vacuum system within the magnet must induce a minimum distortion in the magnetic field. The cavity walls must not contain ferromagnetic materials, which can give rise to strong background signals. Magnetic field modulation used to code the ESR signal must be passed through the walls of the cavity. Thus the cavity wall must be UHV compatible, have a low electrical conductivity, a high thermal conductivity (for purposes of temperature variation), a low magnetic permeability, and have structural integrity.

Our UHV microwave cavity (shown in Figure 2) employs some of the design features as the flow system cavity of Thompson *et al.* ([16]). Even though 35 % of the area of each of the end walls of the cavity is removed, an unloaded Q of 13,000 can be obtained for the TE_{011} mode which is cylindrically symmetric and has a nominal resonant frequency of 9.5 GHz for our cavity dimensions. The large openings in the cavity increase the pumping conductance and decrease errors in pressure measurements. The cavity walls are constructed from 0.020 mil wall titanium. Titanium has a much lower magnetic permeability than stainless steel (1.00005 vs. 1.02) ([17a]), though it has almost the same electrical resistivity ([17b]). Stainless steel also can have a residual ferromagnetism and an earlier stainless steel cavity gave a broad background signal, which could be reduced but not eliminated upon vacuum annealing.

Cavity end pieces are made of macor rings bolted to OFHC copper rings, (cf. Fig. 2) and they prevent leakage of microwave radiation. Since these end pieces are electrically isolated from the rest of the cavity, the TM_{111} mode, which is degenerate with the TE_{011} mode, is suppressed. The two end pieces are connected to non-magnetic subminiature electrical feedthroughs. Thus

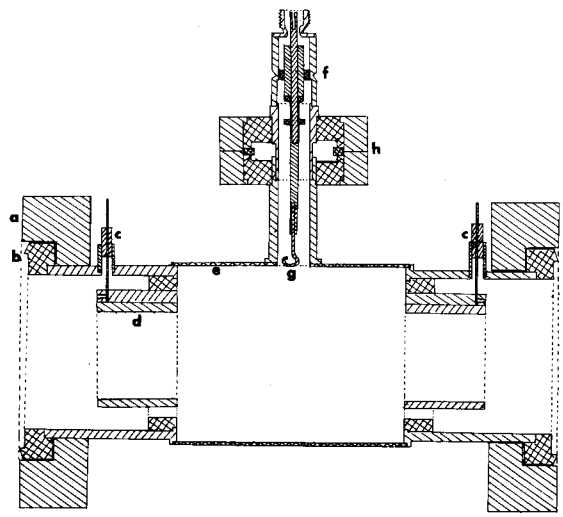

Fig. 2. — UHV-ESR Microwave Cavity consisting of: a) brass backup ring, b) stainless steel knife edge, c) medium voltage feedthrough for static electric field, d) copper/ceramic end ring, e) 0.020 inch titanium walls, f) UHV microwave feed-through, g) coupling loop, h) miniflange assembly.

an electric field can be applied to eliminate an electron cyclotron resonance (ECR) signal (see below).

Microwaves are coupled into the cavity via a wire loop positioned to give maximum coupling to the magnetic component of the microwave rf field for the TE_{011} mode. This loop is connected to a microwave coaxial cable via a high frequency UHV bakeable electrical feedthrough. Since this feedthrough has non-uniform impedance, an OFHC cooper-bead is positioned appropriately on the center conductor to improve cavity coupling. The feedthrough and antenna are connected to the cavity via a miniflange assembly, which allows major adjustments to the cavity coupling at atmospheric pressure; minor adjustments are made with a slide-screw tuner.

The temperature of the cavity is varied from $-150\,^{\circ}C$ to $200\,^{\circ}C$ by flowing preheated or precooled N_2 gas through a teflon jacket around the cavity. The temperature is monitored by a thermocouple epoxied to the cavity wall and it is connected to a circuit regulating the flow of N_2.

A Varian E-12 ESR spectrometer is used for ESR measurements. Magnetic field modulation at a frequency of 25 kHz is used. A drop of 36 % in modulation amplitude is observed with the titanium cavity. This is due in part to attenuation by the walls (the skin depth of titanium is 0.110 inch at 25 kHz) and to a lowering of the Q of the modulation coils due to the presence of the cavity. The modulation coils consist of two pairs of coils mounted on the teflon jacket. The number of windings and size for each pair were adjusted to maximize the magnetic field modulation homogeneity over the dimensions of the cavity.

Copper films were evaporated onto electrolytic polycrystalline copper substrates (c.a. 0.1 mil). The titanium surfaces of the cavity were cleaned under argon before electroplating to remove TiO_2 and improve surface adhesion of the electrolytic copper. 99.999 % copper wire was wrapped around a tungsten filament supported by a stainless steel rod, which is connected to a flange containing the electrical feedthroughs. The assembly is driven into the cavity using a miniature stainless-steel chain-driven bellows assembly. (ESR measurements can only be made when the filament is removed from the cavity). The cavity walls were maintained at 0 °C during evaporation of the Cu. No attempt was made to measure the exact thickness of the deposited film, although the thickness is estimated to be 10^2-10^3 Å based on approximate calibration of the rate of evaporation. Even though the evaporator was outgassed, there was some pressure rise upon evpaoration.

We have measured the sensitivity of our UHV-ESR system using an NBS ruby standard. We found a minimum detectable number of spins of 5×10^{11} spins per gauss linewidth. Our E-12 spectrometer is rated for a sensitivity of 5×10^{10} spins per gauss using the standard Varian cavity. Since the rf magnetic field squared is a factor of 0.16 lower at the walls than at the center of the cavity, our measured value of 5×10^{11} is close to theoretical for a filling factor based upon wall samples. Our cavity has 50 cm^2 of surface area, which gives a sensitivity of 1×10^{10} spins per Gauss for each cm^2 of surface area. Thus for a paramagnetic species with a linewidth of 10 Gauss (linewidths for paramagnetic surface species vary from a few Gauss to hundreds of Gauss), signals should readily be observable for coverages as low as 1 % (S/N $\approx$ 50). We have observed [18] ESR signals with a S/N of 50 for a polyatomic free radical adsorbed on the surface of the cavity at about 10 % monolayer coverage corresponding to about 10^{13} spins/cm^2 (since each molecule has an effective area of ca. 100 $Å^2$). Our UHV-ESR sensitivity may be summarized by the expression:

$$S/N \approx 10^5 \, R\Theta \, \frac{\Delta H_m}{\Delta H^2} F$$

This expression is based on 10^{15} atomic sites/cm^2; for molecules the right-hand side should be divided by the effective area per molecule in $Å^2$ divided by 10 $Å^2$. Also, R is the surface roughness coefficient, Θ is the fraction of a monolayer of radical species and can be greater than unity for more than a monolayer coverage, ΔH_m is the magnetic field modulation amplitude in G. (about 5G. maximum for our system), while ΔH is the derivative ESR linewidth in G. This expression is applicable for $\Delta H_m < \Delta H$. F is the fraction of spins contributing to the particular derivative ESR line and is $\leqslant 1$; e.g. for three equal hyperfine lines characteristic of gaseous NO_2 above several torr., F = 1/3; while for an asymmetric g-tensor the fraction of spins contributing to the most intense peak yields an

$$F \cong (\Delta H / \sqrt{\Delta H^2 + (H_\parallel - H_\perp)^2})^{1/2}$$

where $H_\parallel$ and $H_\perp$ are the field positions of the parallel and perpendicular components respectively. The above expression emphasizes the reduced S/N for broad-asymmetric solid-like signals that are observed on surfaces due to the factor $\frac{\Delta H_m}{\Delta H^2} F$.

Our studies are consistent with a surface roughness factor of order of unity, i.e. the effective surface area including surface roughness is approximately equal to the geometric surface area. (Vacuum evaporation onto surfaces at reduced T $\sim$ 77 °K would be expected to yield a roughness factor of $\sim$ 10-100 due to porosity, but annealing out porous defects in the bulk of the film would occur at more elevated T[19]). We have also successfully used signal averaging to improve signal to noise ratios and resolution by a factor of as much as 10. This is particularly useful for eliminating base-line instabilities which are a problem for broad spectra.

Before we leave the description of the UHV-ESR system, we want to point out that our design permits us to conveniently and rapidly replenish the clean surface film, and to have substantial surface area. Single crystal studies, would, of course, be desirable to permit studies of orientation of surface species as well as reactivity as a function of surface plane. A design wherein a single crystal of metal forms a wall of the cavity would be feasible. However, one would want to be able to remove this wall into another chamber of the UHV system to permit surface cleaning and characterization by conventional UHV methods. This would be an inherently more complicated technique requiring the solution of a number of technical problems. Clearly, it would be valuable to characterize the surface metal films employed in our present technique, by some standard method(s). One such characterization would be the work function of the surface. We have very recently succeeded in performing *in situ* measurement of work function by combining the photoelectric effect with the CREMSEE phenomenon that is explained in the next section, and we might expect further developments along these lines. Other measurements, such as by Auger spectroscopy, would probably require the preparation of surface films in a standard UHV chamber in a manner similar to that employed in the cavity, and this appears to be a reasonable prospect.

We have also employed the basic UHV design of Figure 1 but whith the UHV-ESR cavity replaced with standard UHV tubing onto which a standard ESR spectrosil-quartz sample tube may be attached. This was useful in work with supported metal samples [15]. We are currently extending this concept to evaporate fresh metal films onto the interior surface of a quartz tube while maintaining UHV at this surface. This procedure allows us to use a standard ESR cavity permitting better temperature range, field modulation, and microwave magnetic field. However, it yields lower surface area, reduced pumping conductance, and the quartz is both more gassy and more porous than metal vacuum walls. It also suppresses CREMSEE (see below). We believe this technique is promising for metals with low evaporation temperatures.

III. CREMSEE: Cyclotron Resonance from Microwave Induced Secondary Electron Emission

We observe an intense electron cyclotron resonance (ECR) signal in our UHV-ESR cavity at pressures less than 10^{-2} torr. The signal intensity shows an extremely

non-linear dependence upon microwave power, which can be characterized by a threshold microwave power P_t, below which no ECR signal is observed. P_t is magnetic field dpendent in a manner characteristic of the resonance phenomenon as shown in Figure 3a, a graph of P_t vs. magnetic field. The minimum in P_t (i.e. $P_{t,min}$) occurs at $g = 1.997$. In the text below we shall only consider $P_{t,min}$ in detail and we shall drop the subscript "min" for convenience. The CREMSEE absorption signal (which is readily monitored directly from the crystal detector of the E-12 spectrometer because the signal is so intense) is shown at several microwave powers in Figure 3b and a comparison between the CREMSEE absorption and its first derivative signal (with the latter obtained by conventional ESR detection) just above P_t is shown in Figure 4.

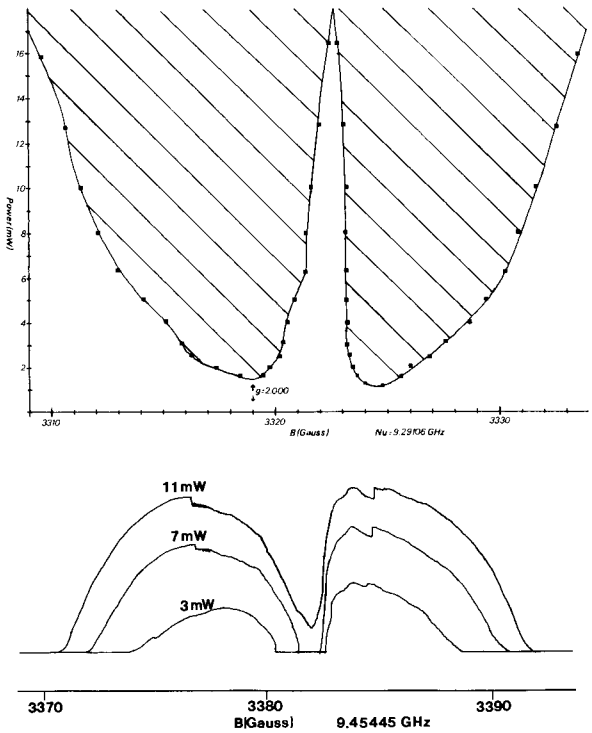

Fig. 3a. — Curve of P_t, the CREMSEE power threshold vs. magnetic field. The shaded region is the domain for which CREMSEE is observed. The surface is air oxidized Cu. b) CREMSEE absorption signal observed for different microwave power levels. The ordinate is not marked; it corresponds to arbitrary units of signal intensity.

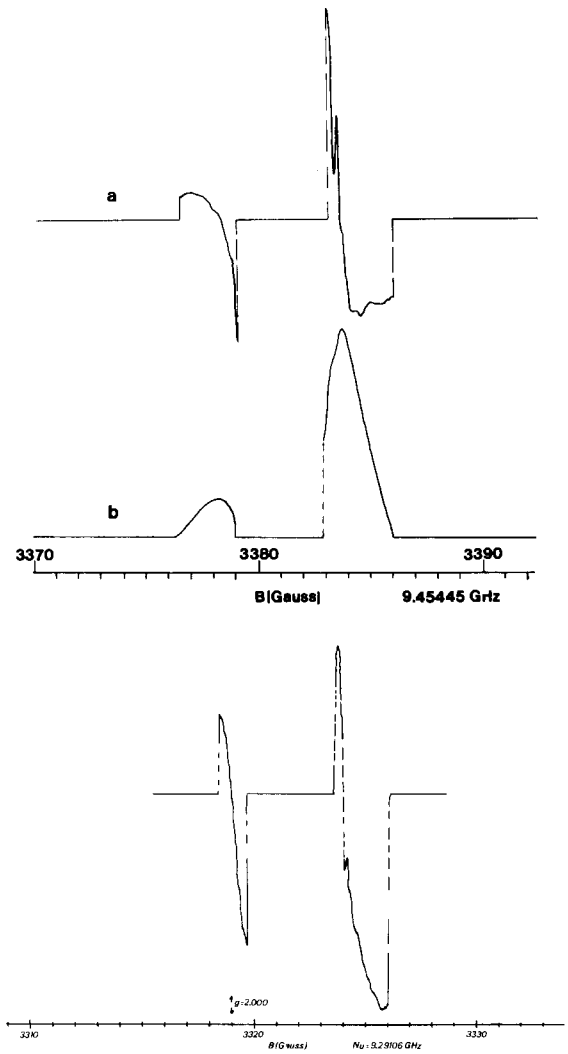

Fig. 4. — ESR spectrum: a) first derivative; b) absorption, of cyclotron resonance of free electrons in a TE_{b11} mode UHV cavity (CREMSEE). Microwave power: 2.1 mW which is slightly above $P_{t,min}$; modulation amplitude: 0.08 Gauss; modulation frequency: 270 Hz; room temperature; pressure: 10^{-9} torr.

The CREMSEE signal is not a simple ECR signal. First of all, there are two distinct absorption signals, a primary absorption with a maximum at $g = 1.9997 \pm 0.0005$ corresponding to $g = 2$ characteristic of ECR, and a secondary (but intense) absorption that is displaced up-field and corresponds to a $g = 1.997$. The primary CREMSEE absorption is fairly symmetric but the secondary absorption is definitely asymmetric, especially near P_t (cf. Fig. 4). The latter exhibits a sharp, nearly-discontinuous rise on its lowfield side. As the power is increased these two absorptions are seen to broaden, and they eventually merge but continue to display central dip (cf. Fig. 3b for P = 11 mW). We estimate as the width of the width of the primary absorption of about 10G from the higher power spectra.

There is a close similarity between the absorption signal vs. magnetic field for higher power (P = 11 mW) displayed in Figure 3b and the shape of P_t vs. magnetic field displayed in Figure 3a. This suggests that there is a close relationship between the intensity of the high power resonance signal and the P_t required to initiate CREMSEE for a particular value of the magnetic field. A further clue to the nature of the phenomenon is found by comparing the CREMSEE absorptions at the different microwave power levels found in Figure 3b. As the power is decreased, the absorption intensity is, of course, decreased. But the lineshape changes may be described in the following manner. As the power is lowered, the shape near the maxima remains nearly the same; one is merely "chopping off" the lower intensity portions of the absorption because they become too weak to sustain the CREMSEE.

The presence of the secondary resonance at $g = 1.997$ is probably due to the fact that the TE_{011} mode has an rf electric field which varies in magnitude and phase across the dimensions of the cavity. We have obtained evidence in support of this in the following manner. A mylar sheet is placed inside the cavity oriented so it is perpendicular to the DC magnetic field and bisecting the cavity into two half-cylinders, (that is, the cylinder axis lies in the mylar plane). This has negligible effect on the cavity mode pattern. In each of these half cylinders the rf electric field components that are

perpendicular to the DC magnetic field (as required to induce ECR) are 180° out of phase with each other. For this case only one absorption, centered at $g = 2$, is observed.

The fact that the CREMSEE signal occurs at $g = 2$ and not at $g = 2.0023$, and it is very intense, indicates that this is an ECR signal, not an ESR signal. The susceptibility for an ECR transition is given by [20]:

$$\chi''_{ECR} = -\frac{N_e e^2}{2m\omega_c} \frac{\tau}{1 + (\omega - \omega_c)^2 \tau^2} \qquad (1)$$

where ω and ω_c are respectively the microwave and the cyclotron resonance frequencies $\left(\omega_c = \frac{eB}{mc}\right.$ in terms of the electric charge e of the electron, its mass m, the velocity of light c, and the magnetic field B), and τ is the mean time between collisions, or in our case is the transit time across the cavity. [We have dropped the contribution of the counter-rotating microwave field component [20a] in Eq. (1), because $|\omega_c \tau| \gg 1$, since τ is of the order of 10^{-8} sec, see below].

The ESR susceptibility is given by [20b]:

$$\chi''_{ESR} = \frac{N_s g^2 \beta^2 \omega_0}{8kT} \frac{T_2}{1 + (\omega - \omega_0)^2 T_2^2} \qquad (2)$$

(where the Larmour frequency $\omega_0 = g\beta BH$ in terms of β the Bohr magneton). In the case that T_2 the transverse spin-relaxation time, is equal to τ, the ratio of susceptibilities for ECR vs. ESR is then given by:

$$\chi''_{ECR}/\chi''_{ESR} = 4\, mc^2\, kT/(\hbar\omega)^2 \qquad (3)$$

This ratio is equal to 3.40×10^{13} for $T = 298\,°K$ and $\omega/2\pi = 9.5$ GHz, and it demonstrates the very high sensitivity for detection of electrons by ECR !

The actual CREMSEE lineshape requires that we modify the expression for χ''_{ECR} to include the facts that (1) the number of electrons depends upon $\Delta\omega \equiv \omega - \omega_c$ i.e. we let $N_e = N_e(\Delta\omega)$ and (2) there is a distribution of transit times τ [represented by normalized distribution function $f(\tau)$]. Thus we write:

$$\chi''_{CREMSEE} = \int N_e(\Delta\omega)\, \hat{\chi}''_{ECR}(\Delta\omega, \tau)\, f(\tau)\, d\tau \qquad (4)$$

where $\hat{\chi}''_{ECR}$ is the ECR susceptibility per electron. When we relate Eq. (4) to the absorption signals shown in Figure 3b (and 4) we conclude that $N_e(\Delta\omega)$ is the function that "cuts off" the low intensity portions of both the primary and secondary ECR signals, and it is clearly also a function of microwave power. Its role is most dramatic just above P_t (cf. Fig. 4) where only a near resonant condition can sustain CREMSEE. The distribution $f(\tau)$ would be expected to lead to a superposition of CREMSEE lines of different width but centered at $g = 1.9997$. [Finally we note that $N_e(\Delta\omega)$ should also be a functional of $f(\tau)$].

When the cavity is biased with a DC electric field, the threshold power P_t increases as shown in Figure 5. The end rings of the cavity are biased with a negative voltage with respect to the cavity walls. Reversing the polarity of the biasing is considerably less effective in increasing P_t. P_t is independent of pressure even down to 10^{-10} torr, while the ECR signal intensity and shape are independent of pressure below 10^{-6} torr. We observe that at 10^{-6} torr, the ECR signal becomes noisy and we see some structure that is dependent upon both pressure and gas composition in a manner we have yet to clarify.

Also, we observe a glow discharge with gas pressure above 10^{-6} torr. But we must have the necessary conditions for CREMSEE (i.e. microwave power above P_t and $\omega \approx \omega_c$). This discharge exists as a beam parallel to the external magnetic field B, and is in the center of the cavity, and about 1/16 inch wide. This width is found to vary as one sweeps the magnetic field through the CREMSEE line but in an irregular fashion. When an external DC field is applied, then the position of the discharge in the cavity also varies in an irregular fashion, but it always remains parallel to B.

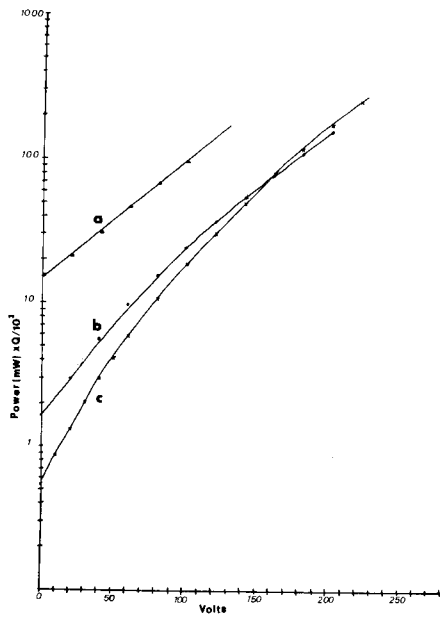

Fig. 5. — Curves of $P_{t,min}$, the CREMSEE power threshold, vs. DC biasing electric field: a) freshly deposited Ag surface; b) air oxidized Ag surface; c) air oxidized Cu surface.

Microwave discharges are, of course, very common in low density gases. They are routinely used to generate H atoms from gaseous H_2, N atoms from gaseous N_2, etc. [21a]. However, this standard technique requires high microwave power (ca. 50 W) into a rather low Q cavity and does not employ a dc magnetic field. We observe discharges of the typical color (e.g. light reddish for H), but we require very small microwave powers $\gtrsim P_t\, 5 \gtrsim$ mW incident on the cavity to sustain the discharge. Given that the conditions for CREMSEE must be fulfilled for our discharges, then we can explain the "high efficiency" of our discharges by recognizing that in CREMSEE the electrons traveling relatively slowly in the direction parallel to B are being highly excited by ECR in orbits perpendicular to this direction; matters discussed more fully below. Thus they should be exceptionally effective in dissociating molecular H_2, O_2, N_2, etc. in the gas phase. [Note also that electrons with a velocity component perpendicular to B, will experience a magnetic force $(= e\vec{v} \times \vec{B})$ leading to orbiting motion about the parallel direction of motion, and this orbiting motion will be further enhanced by the ECR. Thus for these electrons also, it is only the parallel component of v which is unaffected by the ECR]. This also helps to explain the fact that the discharge exists as a beam *parallel* to B. This CREMSEE-induced glow discharge could have some applications in the production of atomic gases when heating effects from large microwave power levels are undesirable.

When the cavity is used in the TE_{112} mode instead of the TE_{011} mode then P_t for CREMSEE increases by a factor of 12 db. This is because the rf electric field perpendicular to the external DC magnetic field is greater for the TE_{011} mode. We have not yet attempted to observe a discharge when the TE_{112} mode is used.

While we next wish to point out the utility of CREMSEE for surface studies with our UHV-ESR system, we do note that its presence can be undesirable while attempting to observe an ESR from a paramagnetic species with a $g \approx 2$. One is readily able to suppress CREMSEE by using a microwave power below P_t or by working with gas pressures above 10^{-2} torr as we have already noted. However, we find that the suppression of CREMSEE by use of the dc electric biasing field, is the most general method, since it automatically permits ESR studies under high vacuum and high microwave power when needed.

As shown in Figure 5, P_t is dependent upon the nature of the metal surface. This fact plus the lack of pressure dependence of the ECR signal below 10^{-6} torr indicates that the source of electrons is from the surface and not from residual gas molecules, so it is not related to the phenomenon observed by Watt, Hand and Schneider [21b], who observed an ECR signal which is non-linear in power but markedly dependent upon gas pressure. (We have confirmed this by covering the metal walls inside the UHV cavity with teflon shetting. No ECR signal was obtained). Instead we believe we are seeing the ECR of secondary electrons emitted from the surface. If electrons can absorb enough successive microwave quanta before collision with either residual gas molecules or the cavity walls, (ca. 100 eV for Cu and Ag), then the secondary electron yield will be greater than unity [22,23]. This leads to electron multiplication until a steady state number of electrons is achieved due to surface charge effects opposing further net emission of electrons. (We estimate that the signal intensity just above threshold corresponds to about 10^3 electrons [24a]. A similar phenomenon known as the multipactor effect or secondary electron resonance [24b] is observed for low pressure, high rf frequency gaseous breakdown and is also attributed to electron multiplication by secondary electron emission. This effect does not involve ECR, so it does not require a dc magnetic field, and it does require some gas being present for its observation. We suspect that the initial or stray electrons, which appear to always be available to initiate the CREMSEE in our experiments, are either due to a few surface electrons that are thermally excited and easily ejected by microwave photons, or else from occasional electrons liberated by cosmic radiation.

We have already pointed out that the absorption of microwaves increases the angular velocity for the orbiting electron but not its linear component parallel to the magnetic field, (i.e. perpendicular to the orbiting plane). This linear component is needed to bring the orbiting electron to the wall. Therefore the slower the linear component, the greater would be the microwave energy absorbed and hence the angular velocity. Upon collision, most of the kinetic energy will be that due to the angular velocity and in a plane approximately parallel to the wall. This configuration is more favorable for increasing secondary electron emission [22,23] than that with electrons with their velocity vector normal to the surface. Our observations of the glow discharge discussed above are consistent with this model. We are currently in the process of developing a quantitative theory based upon these ideas and Eq. 4.

ECR signals observed for free electrons in a vacuum [25] have much narrower linewidths than the signals we observe. This indicates that the secondary electrons we observe have a shorter transit time across the cavity. Our estimated half-width at half-height from Figure 3b of about 4G corresponds to an average transit time of 3.8×10^{-8} sec or a linear kinetic energy of 20eV. This is rather large considering that a majority of secondary electrons are emitted with an energy of 2 to 6 eV [22,23]. However, this estimate of τ must be regarded as crude, since we have not taken the distribution function $f(\tau)$ into our analysis, nor have we fully deconvoluted the ECR lineshape (eq. 1) from Eq. 4 and the spectra of Figure 3b. (Also, we took the transit length as the cavity i.d. of 1.59 inches).

Evidence presented below and from experiments with a stable nitroxide [18] indicates that the microwave threshold P_t is dependent upon chemisorption of gases on the metal surfaces of the cavity. These studies suggest that CREMSEE may be used to measure effects on the surface from chemisorption in a manner analogous to the way work function experiments are currently employed [26]. The advantage of CREMSEE would be the almost order-of-magnitude changes in P_t that we observe (e.g. Fig. 5 and next section) due to CREMSEE, compared to relatively smaller changes typically observed in work function (usually up to 25-50 % changes) [26].

IV. Results of UHV-ESR Study of NO_2 Reactions with Cu Films

With a fresh copper film deposited on the interior of the cavity, no ESR signal is seen. The conduction electron spin resonance of copper is too broad to be observed [27]. When NO_2 is admitted to the cavity at pressures ranging from 10^{-8} torr to 20 torr, no surface NO_2 ESR signal is observed even though NO_2 molecules are paramagnetic [28]. At the higher pressures and/or lower temperatures, multilayer condensation onto the surface can occur. However, NO_2 should be in the form of diamagnetic dimer, N_2O_4 in the condensate [3,29]. Also we do not see any signals characteristic of Cu^{2+} complexes, even though we do for experiments using more conventional techniques: i.e. supported copper (cf. next section) and copper metal experiments under lower vacuum conditions [28a].

We postulated that the "clean" surface prepared under UHV conditions probably lacks some needed additional component(s). At pressures greater than 1×10^{-3} torr gas phase ESR signals are seen for NO_2 and NO but not for O_2. At lower pressures NO_2 and NO can be found with the mass analyzer but again there is no O_2 present. In fact, in pumping the UHV system down to 10^{-7} torr, followed by heating the walls of the cavity, there is marked increase in the peaks on the masse analyzer due to NO, N_2 and NO_2. This is somewhat unusual given that in our experiments with NO_2 under normal vacuum conditions, O_2 is always seen, because of the equilibrium $NO_2 \rightleftharpoons NO + 1/2\ O_2$, which is far to the left [28]. In fact, in these experiments NO is not seen ! We first suspected the lack of O_2 in our UHV experiments, but even when O_2/NO_2 mixtures are used, no surface ESR signal is seen.

A weak Cu^{+2} signal was first observed [28a] for the UHV experiment when extremely large doses of NO_2 were admitted to the cavity. We later found that with mixtures of NO_2 and H_2O, Cu^{2+} signals could be readily observed for condensed multilayers. We have performed experiments with mixtures of NO_2–H_2O ranging from about 40:1 mole ratio to 1:1 mole ratio. The greater the water fraction, the larger is the Cu^{2+} signal, indicating that H_2O is consumed in the reaction and is not just acting as a catalyst.

In particular, when a 1:1 mole ratio of NO_2 and H_2O is used, a very strong Cu^{2+} signal is seen. We describe its evolution below. When this mixture is first condensed onto the copper surface at $-100\ ^\circ C$ and 0.1 torr no ESR signal is observed. When the surface is warmed to

$-80\,^{\circ}C$, a single symmetric ESR signal with $g = 2.177$ and ΔH equal to 110 G is seen. This signal is similar to that observed when NO_2 is first reacted with copper wire under normal vacuum conditions [28a]. Upon further warming, the signal grows quite strong (S/N 500) and a signal due to gas phase NO_2 is observed (c.f. Figure 6; an ESR signal for NO is observed, but at higher fields: 9 KG). Upon pumping off the condensed layer of NO_2/H_2O an anisotropic signal develops which is characterized by: $g_{\parallel} = 2.310$ and $g_{\perp} = 2.100$ and no [63,65] Cu hyperfine structure (hfs). This signal then disappears upon further pumping below 10^{-6} torr at RT.

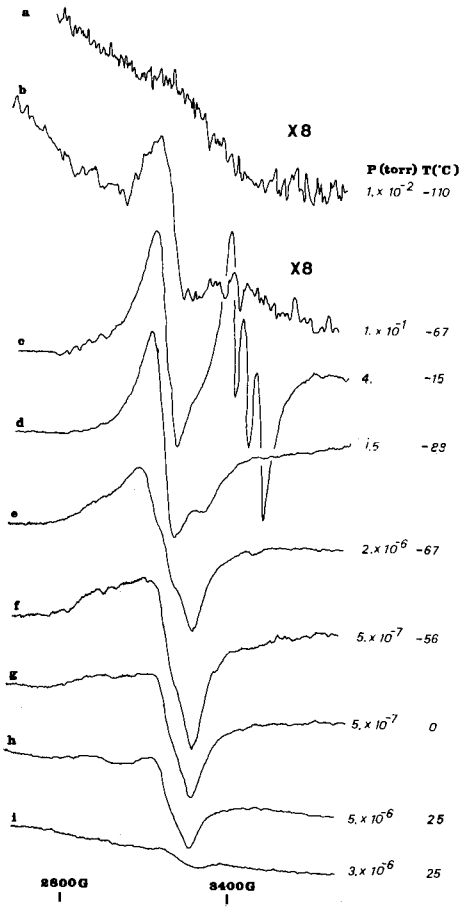

Fig. 6. — ESR spectra for reaction of NO_2 with Cu: a) Initial condensation of NO_2/H_2O mixture; b) and c) surface warmed; d) then recooled with UHV pumps closed off; e) through (i) the cavity is pumped and warmed to remove NO_2/H_2O layer.

Altough the lack of an ESR signal when NO_2 is condensed onto the Cu surface could be explained in terms of dimerization of the NO_2 on the surface, we believe the lack of an ESR signal from NO_2 for our studies with sub-monolayer coverage, for which dimerization is less probable, is due to reaction of NO_2 with the Cu surface. Our conclusion is based on our CREMSEE observations. When NO_2 is leaked in at RT and 10^{-7} torr, the CREMSEE threshold drops to a level near that for an air-oxidized copper surface. NO_2 is probably dissociating on the surface to form surface oxide and NO. This is supported by our observation of NO (but not O_2) with the mass analyzer at low pressures and by ESR at higher pressures. Although NO is paramagnetic, we do not see any surface ESR signal from adsorbed NO even when pure NO is leaked into the vacuum system with clear (or oxidized) Cu. We believe this is due to the formation of a diamagnetic surface complex [3] (with pure Cu) or to a diamagnetic dimer [30]. Also, we note that UPS and XPS studies [29] and IR studies [3] of NO and NO_2 adsorbed on nickel surfaces yield similar results whether either NO or NO_2 is adsorbed, which implies that NO_2 dissociates to NO. At higher pressures and/or lower temperatures physisorbed multi-layers of NO_2 can also exist, and the NO_2 should dimerize to give N_2O_4, which can self-ionize [31] to a small extent to give $NO^+NO_3^-$. NO^+ can oxidize copper to give nitrate species and NO [32]. Surface nitrate species have been observed [3,29] when nickel is exposed to saturation dosages of NO_2. Thus NO_2 and N_2O_4 can be expected to react with copper to give oxide and nitrate species, respectively with the production of NO. It is likely that the oxide formation is the primary step as judged by the absence of any O_2 in the UHV experiment. Its presence in the ordinary vacuum experiments is likely indicative of the fact that the surface layer is already an oxide, (which, however, can still react with NO_2).

While $CuNO_3$ and Cu_2O are diamagnetic species, CuO and $Cu(NO_3)_2$ are paramagnetic and should give some kind of ESR signal. We have shown by conventional ESR experiments that bulk CuO, $Cu(NO_3)_2 \cdot N_2O_4$, and $Cu(NO_3)_2$ all give structureless signals with g factors equal to 2.308, 2.142, and 2.147 and linewidths of 1,000 G., 320 G., and 480 G. respectively. The CuO signal is symmetric, while the copper nitrate signals are asymmetric. Thus a magnetically concentrated monolayer of CuO or $Cu(NO_3)_2$ might give too broad and hence too weak a signal to observe. Monomeric $Cu(NO_3)_2$, on the other hand, gives a well-resolved ESR signal [33], which is very similar to what we observe for the reaction of Cu/vycor with NO_2, [28a] (cf. next section).

The appearance of a Cu^{+2} signal when H_2O is present is most likely due to the formation of HNO_3 [34] :

$$2NO_2 + H_2O \rightleftharpoons HNO_3 + HNO_2$$

$$3HNO_2 \rightleftharpoons HNO_3 + 2NO + H_2O$$

In addition any free NO_2 is nearly completely ionized to $NO^+NO_3^-$ and HNO_3 is actually a mixture of free acid, acid anhydrate, and water [34a].

$$2HNO_3 \rightleftharpoons N_2O_5 + H_2O$$

Thus HNO_3 and H_2O should readily solvate any copper surface species to give hydrated copper nitrate species of the form, $[Cu(H_2O)_{6-n}(NO_3)_n]^{2-n}$. We have found that the ESR spectra from aqueous copper nitrate are similar to those observed in the UHV system with NO_2 H_2O (cf. Table 1b). $Cu(NO_3)_2$ in H_2O at $90\,^{\circ}K$ gives a symmetric ESR signal with $g = 2.169$ and $\Delta H = 175$ G, and may be attributed to the octahedral hexaquo species $[Cu(H_2O)_6^{+2}]$, which is expected to exhibit dynamic Jahn-Teller effects [34b].

When nitric acid is added an asymmetric signal with $g_{\parallel} = 2.376$, $g_{\perp} = 2.074$, and $g_{ave} = 2.175$ develops which we attribute to a tetragonal hydrated copper nitrate species [e.g. $Cu(H_2O)_4(NO_3)_2$ or $[Cu(H_2O)_2(NO_3)_4]^{-2}$]. While [63,65] Cu hfs is seen for dilute frozen solutions of $Cu(NO_3)_2$ in nitric acid, and for the signals observed from supported Cu (cf. next section), the lack of hfs in the UHV Cu^{+2} signals is due to exchange narrowing and is characteric of magnetically concentrated systems. For example bulk $Cu(NO_3)_2.2.5H_2O$ shows g anisotropy ($g_1 = 2.335$, $g_2 = 2.133$, and $g_3 = 2.082$) but no copper hfs. The average g values for Cu^{+2} complexes observed in the UHV experiment and for aqueous copper nitrate species range between 2.169 and 2.183. These are characteristic

TABLE 1a

ESR Parameters of ^{63}Cu (II) ion complexes supported on Vycor (This Work)

Cu(II) complex	Hyperfine ($cm^{-1} \times 10^{+4}$) $A_\parallel$	$A_\perp$	g-factor $g_\parallel$	$g_\perp$	g_{ave}	Temp.	System
Type I	168.8	-	2.292_1	2.052	2.132	-196°C	Cu^{2+}/Vycor after evacuation at RT for several hours. Removed by adding NO_2.
Type I'	156	-	2.301	2.039	2.126	-120°C	NO_2 added to Cu^{2+}/Vycor after heat treating at 10^{-6} torr and then partial reduction by H_2 at 150°C.
Type II	147.8(±1.4)	-	2.363_4	2.052	2.156	-196°C	Formed from Type I when NO_2 added to Cu^{2+}/Vycor.
Type II'	140.6		2.361_3	2.038_9	2.146	-120°C	NO_2 added to Cu^{2+}/Vycor after evacuating and treating with 1 atm. H_2 at 150°C.
Type II"	145.6(±2.7)	19.6 ± 2.4	2.344_7	2.049_0	2.148	RT	NO_2 added to Cu^{2+}/Vycor after evacuation at 500°C.
Type II'''	143.6	12.5	2.3400	2.0600	2.1533	-196°C	(Same conditions as for Type III)
Type III	180.1(±1.3)	20.2	2.279_0	2.059_0	2.132_3	-196°C	NO_2 added to H_2 reduced (at 500°C) Cu metal/Vycor.
Type IV	< ΔH		g_{iso} = 2.1596 ΔH = 250 to 420G (65°C) (-140°C)				Partial reduction of Cu^{2+}/ Vycor in presence of H_2 (at 400°C).

TABLE 1b

ESR Parameters of ^{63}Cu (II) Ion Complexes

			^{63}Cu Hyperfine ($cm^{-1} \times 10^{+4}$) $A_\parallel$	$A_\perp$	$g_\parallel$	$g_\perp$	g_{ave}	Temp. °K	Symmetry
$Cu(H_2O)_6^{2+}$	This work	Water	-	-	Isotropic: 2.169			90	Octahedral (on average) ΔH = 175G.
$Cu(H_2O)_{6 \text{ or } 4}^{2+}$	(1)	Zeolite	133	21	2.37	2.07	2.17	77	Octahedral with tetragonal distortion.
$Cu(H_2O)_4^{2+}$	(2)	Silicate Layer	175	-	2.33	2.08	2.16	77	
$Cu(H_2O)_{6-n}(NO_3)_n^{2-n}$	This work	Nitric Acid	156	-	2.376	2.074	2.175	77	
$Cu(NO_3)_2$	(3)	Oriented Neon matrix	190	16.7	2.2489	2.0522	2.118	4	Close to square planar.
Cu^{2+} bisacetylacetonate	(4)	$Pd(C_5H_7O_2)_2$	160	19.7	2.266	2.053	2.124	77	
$Cu(NH_4)_4^{2+}$	(1)	Zeolite	184	-	2.25	2.04	2.11	77	
$Cu(C_5H_5N)_4^{2+}$	(1)	Zeolite	193	-	2.24	2.03	2.10	77	

1) C. M. Naccache and Y. Ben Taarit, Chem. Phys. Lett. 11, 11 (1971).

2) D. M. Clementz, T. J. Pinnavaia, and M. M. Mortland, J. Phys. Chem. 77, 196 (1973).

3) P. H. Kasai, E. B. Whipple, and W. Weltner, J. Chem. Phys. 44, 2581 (1966).

4) A. H. Maki and B. R. McGarvey, J. Chem. Phys. 29, 31 (1958).

of Cu^{+2} coordinated by oxygen atoms in an octahedral or near octahedral arrangement (cf. Table 1b).

Since the hydrated copper nitrate species can readily be desorbed into the condensed layer, further reaction by NO_2 or $N_2O_4(NO^+NO_3^-)$ can occur. This is consistent with our observation of a dramatic increase in signal intensity above -30 °C. HNO_3 does not actually react with the metal surface (35a), but acts to solvate Cu^{+2} surface species and is a source of H_2O to hydrate these species.

Thus we believe the initial ESR signal observed in the UHV system is due to the formation of an octahedral hydrated copper nitrate species which is reduced to tetragonal symmetry upon pumping the condensed multilayer. Although the symmetric signal could be attributed to a rotating species of low symmetry, the lack

of expected temperature dependence of this signal precludes this possibility. Finally the disappearance of the Cu^{+2} signal upon further pumping is attributed to decomposition of the hydrated copper nitrate due to the loss of HNO_3 ([35b]). In fact, the Cu^{2+} ESR signal cannot be regenerated by addition of NO_2 unless H_2O is also leaked in.

V. NO_2 on Cu Supported on Vycor

An important objective of UHV surface experiments is to serve as the basis for a better understanding of the reactive and catalytic properties of "real" surfaces. We therefore performed a study of the interaction of NO_2 with Cu supported on crushed vycor for purpose of comparison ([36]).

The Vycor was prepared and activated in the same manner as Clarkson ([37]). It was immersed in 0.05-0.1 M aqueous solution of $Cu(NO_3)_2 \cdot 3H_2O$. The mixture is allowed to stand for 24 hours at RT, then filtered and dried overnight. The sample is then evacuated at ca. 10^{-6} torr, and then reduced under 1 atm of H_2 at 500 °C to produce supported Cu metal. The formation of Cu metal was confirmed by the red-pink color of the sample and no ESR signal due to Cu^{2+}; (the color of Cu^{+} should be brown or white) ([38]). We used an arrangement for the ESR studies such that the sample tube remained attached to the vacuum line, while the sample was inserted in a conventional ESR cavity. This permitted *in situ* ESR observations as the NO_2 gas was admitted. After exposing the sample to NO_2 with 0.1 – 1 torr pressure at room temperature, the sample color quickly changed to blue-gray implying that the Cu on Vycor is being oxidized by NO_2. At the same time a well-resolved ESR spectrum of ^{63}Cu appeared.

The ESR spectrum (cf. Fig. 7) shows two types (II and III) of Cu^{2+} complexes, and the hyperfine and g-tensors appear in Table 1a. Based on the ESR parameters given in Table 1b and discussed in the previous section we assign Type II to the octahedral with tetragonal distortion structure (formed from initially unreduced Cu^{2+}, see below) and Type III to the square planar structure. We observe still another Cu^{2+} spectrum (Type I) (cf. Fig. 8) when we look at the original Cu^{2+}/Vycor after it is evacuated but prior to any reduction or addition of NO_2. It is readily converted to Type II just by addition of NO_2 showing that type II is formed by an exchange and/or addition of ligands as opposed to any oxidation of the Cu^{2+}. This type I spectrum has ESR parameters that are close to those of square planar. [Other variations of types I and II are seen under conditions summarized in Table 1a, (see also Fig. 8). Also one observes that the type I spectrum is transformed into a single broad line (Type IV) by partially reducing the Cu^{2+}/Vycor at 400 °C in an H_2 atmosphere; this could be due to a highly symmetric (octahedral) complex or to cluster formation] ([39]).

We want, at this point, to emphasize that virtually all the Cu^{2+} spectra we observe, i.e. Types I, II, and III, we atrribute to monodispersed adsorbed atomic Cu as distinguished from oxidized crystallites of copper. We do not believe that this conclusion is in conflict with the observation (cf. present work and ref. 38) that most of the copper is in the form of metallic cyrstallites. Some reasonable fraction of the copper present may be expected to be in the form of monodispersed adsorbed atomic Cu, probably bonded covalently, via the oxygen atoms, to the silica surface. There is, in fact, theoretical ([40]) as well as experimental ([41,42]) evidence to support this point of view. One naturally expects such surface

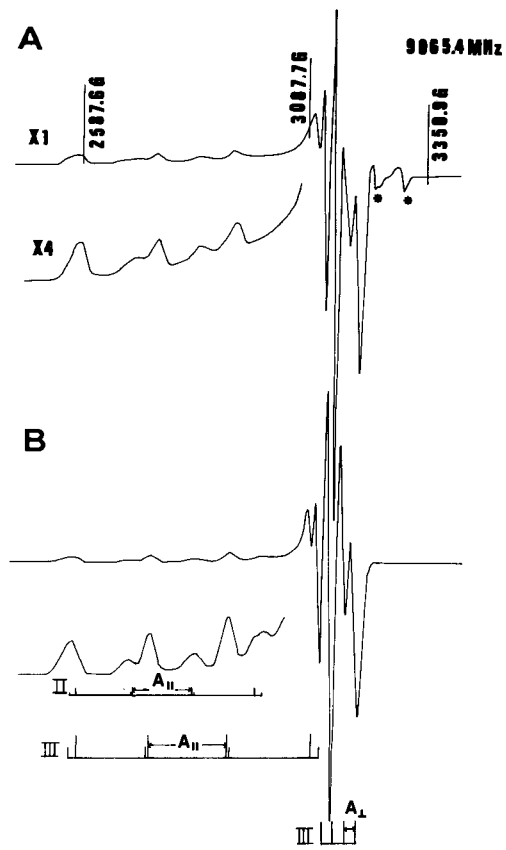

Fig. 7a). – ESR spectrum obtained after exposing the copper metal supported on Vycor to 1 torr NO_2 at room temperature followed by cooling to 93 °K. This spectrum corresponds to the type III Cu^{2+} complex together with a weak spectrum due to the type II Cu^{2+} complex (cf. Table 1a).

Fig. 7b). – Computer Simulated Spectrum using Type III and Type II''' parameters given in Table 1a. The ratio of III to II''' used was 2:1. Included are the contributions from ^{63}Cu (69 % abundance) and ^{65}Cu (31 % abundance). The hyperfine parameters for ^{65}Cu are 1.071 times those for ^{63}Cu given in Table 1a. [The intrinsic linewidths are angular dependent according to: $T_2^{-1} = (T_{2,\parallel})^{-1} \cos^2\theta + (T_{2,\perp})^{-1} \times \sin^2\theta$. For Type III, $(T_{2,\parallel})^{-1} = 14$ G. and $(T_{2,\perp})^{-1} = 6.5$ G, while for Type II''' they are 17 G and 12 G. respectively].

bonded Cu atoms to exhibit chemically different properties than the metallic Cu crystallites because of i) effects of bonding to the silica and ii) absence of conduction band-electron delocalization.

We can rationalize our ESR spectra only in terms of distinct Cu species, because they exhibit well-resolved hfs characteristic of magnetically dilute Cu^{2+} complexes (cf. above discussion). The Cu^{2+} spectra one would obtain from crystallites of Cu^{2+} complexes would have no hfs, because of exchange-narrowing, just as we reported in the previous section for the UHV films (and for Cu metal). When we consider atoms vs. small clusters, we first note that dimers of Cu^{2+} complexes are known to give markedly different ESR spectra ([43]), the features of which can be generalized to trimers, etc. showing how the spectrum soon loses resolved hfs.

However, we have noted the color change of the sample to blue-gray, implying that the Cu crystallites are being oxidized by the NO_2. But, we do not observe any ESR spectrum due to such oxidized Cu crystallites. It appears to us that this oxidation process is similar to that which we observed for the UHV-Cu films in contact with NO_2 but in the absence of H_2O ([44]), so the possible reasons for non-observation of an ESR signal should be much the same.

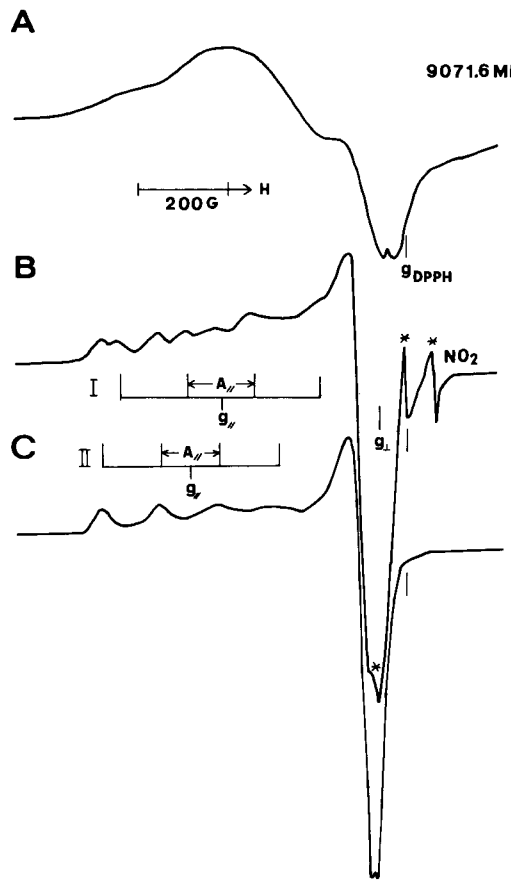

Fig. 8. — ESR spectra of copper Cu $(NO_3)_2$ supported on Vycor after evacuating and treating with 1 atm. H_2 at 150 °C. A) and B) are spectra recorded at — 120 °C before and after the admission of 3 torr NO_2 respectively. The spectrum C) was recorded at — 120 °C after first warming to room temperature and evacuating for 12 hours to remove excess NO_2. An anisotropic triplet marked with* corresponds to NO_2 adsorbed on Vycor. Also g_{DPPH} corresponds to the g-value of DPPH (g = 2.0036). The co-existence of the two types of Cu^{2+} formed: I and II is shown in spectrum B.

Thus, in comparing the results on the vycor support to those obtained in the UHV-ESR experiments, we note that the only signals seen in the latter case are due to hydrated Cu^{2+} complexes. While these are from magnetically concentrated Cu^{2+} complexes, we judge from their g-tensors that they may be somewhat similar to type II species seen on the vycor support, but from magnetically dilute Cu^{2+} complexes. The similar but non-identical g-tensors suggest to us that chemisorbed OH (44) on the silica is likely playing an important role for Type II signals, but structural details of the Cu^{2+} complexes monodispersed on silica are not quite the same as those formed on the metallic crystallites. The absence of any signal from the UHV-ESR experiment that could be attributed to magnetically concentrated type III would then be because either this species can only be formed from Cu atoms dispersed on the support, or else that when magnetically concentrated, it gives a very broad signal which would be very difficult to observe, [e.g. Cu $(NO_3)_2$, cf. previous section].

We believe that a better understanding of the reactivity of supported Cu can be achieved by performing UHV experiments in which a clean (metal) oxide support surface is first prepared (under UHV conditions) and then Cu is deposited in a fractional monolayer. Such experiments appear to be feasible by our methods and we are in the process of developing them.

IV. Conclusions

1) We have developed a technique whereby high sensitivity UHV-ESR experiments may be performed on clean metal and oxide surfaces.

2) We have observed and characterized the new phenomenon of CREMSEE. We have also shown that it is a sensitive indicator of surface bonding even when conventional ESR signals are absent.

3) We have analyzed in detail the reaction of NO_2 with clean Cu surfaces. We find that only in the presence of H_2O is there a distinct Cu^{2+} ESR signal characteristic of a symmetry site that is octahedral but with tetragonal distortion. The surface paramagnetism is magnetically concentrated and shows micro-crystalline characteristics. The initial oxidation of Cu by NO_2 can be monitored by the reduction in CREMSEE threshold power even though there is no conventional ESR signal. UHV clean conditions were needed to correctly determine the nature of the reactions.

4) From a comparison of results with supported Cu under normal vacuum conditions it is shown that for supported Cu, mono-dispersed supported Cu atoms are readily oxidized by NO_2 to form a Cu^{2+} complex with symmetry close to square planar that is not seen in the UHV-ESR experiments.

5) It is believed that a combination of well-designed UHV-ESR, to monitor paramagnetic surface sites and gas phase ESR species, CREMSEE, to detect surface bonding, and UHV Mass Analyzer techniques will prove very useful in studying reaction mechanisms on metal surfaces and on supported metals on oxide surfaces. Such studies can be amplified by future developments such as the use of CREMSEE to measure work functions (45). Results from these studies can then be compared with those on "real" surfaces and with conventional reactions in the bulk.

Acknowledgements

We wish to thank Professors R. P. Merrill, J. M. Blakely, and T. N. Rhodin for their advice on UHV techniques, and Drs. Y. Kera and C. T. Yu for their help in the early stages of this project. This research was supported by Grant No. DE-AC02-80ERO4991 from the Office of Basic Energy Sciences of the DOE, by the Cornell Materials Science Center (NSF), and acknowledgement is made to the Donors of the Petroleum Research Fund, administered by the American Chemical Society, for partial support (Grant No. 10935-N5).

References

(1) **C.S. Fadley.** — In *Electron Spectroscopy: Theory, Techniques, and Applications,* Vol. 2, eds. C.R. Brundle and A.D. Baker, London, Academic Press, 1978.

(2) **B.A. Sexton.** — *J. Vac. Sci. Technol.,* 1979, **16**, 1033.

(3) **B.A. Morrow and L.E. Moran.** — *J. Catal.,* 1980, **62**, 294.

(4) **T. Takenaka.** — *Adv. Colloid Interface Sci.,* 1979, **11**, 291.

(5a) **A.M. Bradshaw and F.M. Hoffmann.** — *Surface Sci.,* 1978, **72**, 513.

b) **P.R. Mahaffy and M.S. Dignam.** — *Surface Sci.,* 1980, **97**, 377.

c) **R.B. Bailey, T. Iri and P.L. Richards.** — *Surface Sci.,* 1980, **100**, 626.

(6) **T.H. Wood and M.V. Klein.** — *J. Vac. Sci. Technol.,* 1979, **16**, 459.

(7) **J.H. Lunsford.** — *Cat. Rev.,* 1973, **8**, 135.

(8) **D. Haneman.** — In *Characterization of Solid Surfaces,* Eds, P.F. Kane and G.B. Larrabee, Plenum, 1974, Ch. 14.

(9) G.L. Gardner and E.J. Casey. – *Cat. Rev.*, 1974, **9**, 1.
(10) *Magnetic Resonance in Colloid and Surface Sciences*, Eds. H.A. Resing and C.G. Wade, ACS Symposium Series, 1976, 34.
(11) R.B. Clarkson and S. McClellan. – *J. Catal.*, 1980, **62**, 551, and references therein.
(12) B.P. Lemke and D. Haneman. – *Phys. Rev. Lett.*, 1975, **35**, 1379.
(13) P. Svejda. – *Rev. Sci. Instrum.*, 1977, **48**, 1092.
(14) P.A. Thomas, M.H. Brodsky, D. Kaplan and D. Lepine. – *Phys. Rev. B*, 1978, **18**, 3059.
(15) M. Shiotani, G. Moro and J.H. Freed. – *J. Chem. Phys.*, 1981, 74, 2616.
(16) M.C. Thompson, Jr., F.E. Freethey and D.M. Waters. – *IRE trans. Microwave Theory and Tech.*, MTT-7, 388, 1959.
(17a) *Metals Handbook*, 8th Ed. Vol. 1, ed. Taylor Lyman, American Society for Metals, 1961, pp. 422 and 1225.
(17b) *CRC Handbook of Chemistry and Physcis*, 54th Ed., ed. R. Weast, CRC Press, 1973, p. 150.
(18) M. Nilges and J.H. Freed. – *Chem. Phys. Lett. in press*, Sept. 1, 1981.
(19) J.A. Allen and J.W. Mitchell. – *Disc. Far. Soc.*, 1950, **8**, 309.
(20a) K.G. Mothes, E. Schutes, and R.N. Schindler. – *J. Phys. Chem.*, 1972, **76**, 3758.
(20b) A. Abragam. – *Principles of Nuclear Magnetism*, Oxford University Press, New York, 1961.
(21a) A.A. Westenberg and N. de Haas. – *J. Chem. Phys.*, 1969, **50**, 707.
(21b) F. Watt, J.W. Hand, E.E. Schneider. – *J. Phys. A.*, 1971, 4, L25.
(21c) Added in proof: F. Hughes and F.W. Patten [Mol. Phys., *9*, 233 (1965)] have observed somewhat similar signals from the surface of an insulator inserted in an evacuated cavity, but no signal was observed from the empty evacuated cavity.
(22) O. Hachenberg and W. Brauer. – In *Advances in Electronics and Electron Physics*, XI, ed. L. Marton, Academic Press, 413, 1959.
(23) D.J. Gibbons. – In *Handbook of Vacuum Physics*, ed. A.H. Beck, Pergamon Press, Vol. 2, 1966.
(24a) The power absorbed during CREMSEE may be measured directly with a microwave power meter. One measures the change in reflected power on and off resonance. Just above P_t we obtain roughly a μWatt CREMSEE absorption. This translates into number of electrons from $P = \omega \chi''_{ECR} \overline{E_1^2}/2$, where $\overline{E_1^2}$ is an average over the cavity and $\tau \sim 1.5 \times 10^{-8}$ sec. see below.
(24b) A.J. Hatch and H.B. Williams. – *Phys. Rev.*, 1958, **112**, 681.
(25a) S.C. Srinivasan and J.E. Willard. – *J. Chem. Phys.*, 1973, **59**, 1701.
(25b) W.C. Elmore. – *Am. J. Phys.*, 1975, **43**, 305.
(26) J.L. Gland and G.A. Somorjai. – *Adv. in Colloid and Interface Sci.*, 1976, **5**, 205.
(27) D. Lubzens, M.R. Shanabarger and S. Schultz. – *Phys. Rev. Lett.*, 1972, **29**, 1387.
(28a) M. Nilges, M. Shiotani, C.T. Yu, G. Barkley, Y. Kera and J.H. Freed. – *J. Chem. Phys.*, 1980, 73, 588.
(28b) M. Shiotani and J.H. Freed. – *J. Phys. Chem.* (submitted).
(29) C.R. Brundle. – *J. Vac. Sci. Technol.*, 1976, **13**, 301.
(30) S. Furuyama, T. Morimoto and R. Hirasawa. – *J. Phys. Chem.*, 1978, **82**, 1027.
(31) C.C. Addison. – In *Chemistry in Non-aqueous Ionizing Solvents*, Vol. 3, Part 1, eds. G. Jander, M. Spandau, and C.C. Addison, Pergamon Press, 1967.
(32) C.C. Addison and N. Logan. – *Adv. Inorg. Chem. Radiochem.*, 1964, **6**, 71.
(33) P.H. Kasai, E.B. Whipple and W. Weltner. – *J. Chem. Phys.*, 1966, **44**, 2581.
(34a) W.H. Lee. – In *The Chemistry of Non-Aqueous Solvents*, ed. J.J. Lagowski, Vol. 2, Academic Press, 1967.
(34b) A. Abragam and B. Bleaney. *Electron Paramagnetic Resonance of Transition Ions*, Oxford University Press, New York 1970.
(35a) A.G. Repa and L.M. Guzhavina. – *J. Appl. Chem. USSR*, 1952, **25**, 1333.
(35b) R. Schubert. – *J. Electrochem. Soc.*, 1978, **125**, 1114.
(36) See: D.M. Clementz, T.J. Pinnavaia and M.M. Mortland. – *J. Phys. Chem.*, 1973, 77, 196, and references therein for previous studies of Cu (II) ESR on a variety of supports.
(37) R. Clarkson and A.C. Cirillo. – *J. Vac. Sci. Technol.*, 1972, **9**, 1073 ;
R. Clarkson and J. Turkevich. – *J. Colloid. Interface Sci.*, 1972, **38**, 165.
Varian Application Note EPR 77-1, 1977.
(38) Our method of sample preparation and reduction is very similar to that of Naccache and Been Taarit [*J. Catal.*, 1971, **22**, 171], who studied copper Y zeolites. They also observed the same color changes upon H_2 reduction and confirmed the formation of copper metal crystals by chemical analysis and X-ray diffraction. They noted that CO-reduced samples are reduced to cuprous ions.
(39) We also observe the species $^{14}NO_2^{2-}$ adsorbed on Vycor [cf. J.H. Freed, DOE Report No. COO-4991-1, 1979]. One possible reaction forming NO_2^{2-} may be: $O^{-2} + NO \rightarrow NO_2^{-2}$.
(40) R.C. Baetzold. – *J. Phys. Chem.*, 1976, **80**, 1504.
(41) J.R. Katzer, G.C.A. Schuit and J.H.C. van Hooff. – *J. Catal.* 1979, **59**, 278.
(42) R.R. Cavanagh and J.T. Yates. – *Jr., J. Chem. Phys.*, 1981, **74**, 4150.
(43) A. Abragam and B. Bleaney. *Electron Paramagnetic Resonance of Transition Ions*, Oxford University Press, NY, 1970, pp. 506-509.
(44) It is known that water molecules are formed by the reduction process using H_2 (cf. ref. 38). That is:

$$H_2 + O^{2-} \rightarrow H_2O + 2e^-$$

$$(2e^- + Cu^{2+} \rightarrow Cu^0)$$

Therefore, we have been very careful to take all the known precautions to remove H_2O from the system. Our procedures (cf. text above) were as follows: 1) in the course of reduction, we used the generally accepted method of a liquid nitrogen cold trap to collect the H_2O formed, then 2) after the reduction we continuously evacuated the sample at ca. 10^{-6} torr at 500 °C for several hours to remove H_2O and H_2. Finally, as noted above, the sample tube remained an integral part of the vacuum system even during exposure to NO_2. However, it is known to be difficult to effectively remove hydroxyl groups bonded to the surface.
(45) M. Nilges and J.H. Freed. – (Unpublished results).